Acta Materialia 204 (2021) 116494

Contents lists available at ScienceDirect

Acta Materialia

journal homepage: www.elsevier.com/locate/actamat

Full length article

Ultra-high strength and plasticity mediated by partial dislocations and defect networks: Part II: Layer thickness effect

Ruizhe Su[a], Dajla Neffati[b], Qiang Li[a], Sichuang Xue[a], Cuncai Fan[a], Jaehun Cho[a], Yifan Zhang[a], Jin Li[a], Haiyan Wang[a], Yashashree Kulkarni[b], Xinghang Zhang[a,*]

[a] School of Materials Engineering, Purdue University, West Lafayette, IN, 47907, USA
[b] Department of Mechanical Engineering, University of Houston, Houston, TX, 77204, USA

ARTICLE INFO

Article history:
Received 30 March 2020
Revised 6 November 2020
Accepted 14 November 2020
Available online 20 November 2020

ABSTRACT

Layer thickness dependent mechanical behaviors of metallic nanolaminates have been extensively investigated. In a recent study [1], we show that a particular defect network, consisting of layer interface, stacking faults and twin boundaries, plays an important role in achieving high strength in Cu/Co multilayers. Here, we report a follow-up study on the effect of layer thickness on this unique interplay of defect networks. To this end, we investigate the mechanical behavior of highly textured Cu (111)/Co (0002) multilayers with individual layer thickness of 5, 25 and 100 nm. *In situ* micropillar compression tests show that the Cu/Co 25 nm multilayers have a much higher strength than 100 nm and 5 nm multilayers. Post-deformation TEM analyses and MD simulations reveal the layer thickness dependent variations of defect density dominating the strengthening effect in multilayers. This study provides new perspectives on optimal defect networks for the design of high strength, deformable metallic materials.

1. Introduction

Metallic multilayers have been extensively studied due to their superior properties including high strength, good magnetic properties and radiation tolerance, and have applications in wear resistant coatings, semiconductor devices, hydrogen storage and microelectromechanical systems (MEMS) [2–33]. The mechanical properties of multilayers show prominent layer thickness dependence [34]. When the individual layer thickness (h) is greater than 50 nm, the major deformation mechanism is the pile-up of dislocations against the layer interface, following the Hall-Petch relationship [34]. When h is in the range of 5-50 nm, dislocation pile-up becomes difficult due to limited thickness of the layers. Consequently, confined layer slip (CLS) becomes the dominant deformation mode. Peak hardness is often reached when h is below 5 nm, and softening is sometimes observed in multilayer systems when h decreases to 1~2 nm [2,13,15,34]. In addition to layer thickness, the microstructure of multilayers, such as grain size, defects and the nature of layer interfaces, all play an important role in tailoring the mechanical behavior of multilayers [10,12,13,18,35]. Our recent study on Cu/Co 25 nm multilayers [1] shows that the Cu (111)/Co (0002) multilayer with FCC/HCP interface has much higher strength than the Cu/Co multilayers with FCC/FCC interface even though they have identical layer thickness. Coherent twin boundaries (CTBs) in Cu, stacking faults (SFs) in Co and FCC/HCP incoherent layer interface form a unique defect network, and collaboratively enhance the strength and deformability. However, it is unclear if layer thickness can tailor the formation of defect networks and the corresponding strengthening mechanisms.

Here we report a systematic follow-up study of highly textured Cu/Co multilayers with three different layer thickness, specifically, 5, 25 and 100 nm, using *in situ* compression tests. Transmission electron microscopy (TEM) studies show that when h is 100 nm, localized deformation in Cu layer occurs due to the lower density of CTBs. When h decreases to 5 nm, molecular dynamics (MD) simulations and high resolution TEM studies reveal that the Cu/Co interface becomes coherent. Shockley partial dislocations can transmit through the coherent layer interface, leading to softening. Thus, maximum strength is achieved in Cu/Co 25 nm multilayer with the defect network comprising CTBs, SFs and incoherent FCC/HCP interfaces.

2. Experimental and simulation methods

2 μm thick Cu/Co multilayer films with different layer thickness (h = 5, 25 and 100 nm) were deposited on HF etched Si (110) substrates using DC magnetron sputtering. The base pressure of the sputter chamber was 5×10^{-6} Pa and the deposition rates were

* Corresponding authors.
E-mail address: xzhang98@purdue.edu (X. Zhang).

https://doi.org/10.1016/j.actamat.2020.116494
1359-6454/

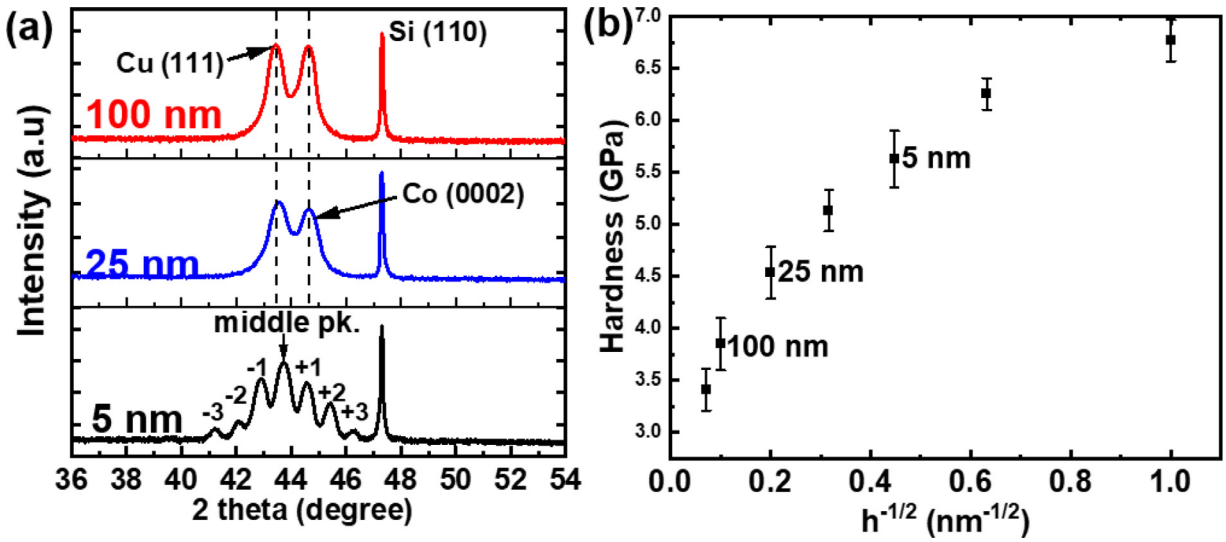

Fig. 1. (a) XRD profiles of 2-μm thick Cu/Co 25 nm and Cu/Co 100 nm multilayers on Si (110) substrate reveal strong Cu (111) and Co (0002) texture. The Cu/Co 5 nm multilayer has prominent satellite peaks arising from the superlattice. (b) The nanoindentation hardness of Cu/Co multilayers increases with decreasing layer thickness.

~0.5 nm/s for Cu and ~0.15 nm/s for Co respectively. X-ray diffraction (XRD) experiments were performed by using a Bruker D8 Discover X-ray powder diffractometer at room temperature. TEM and HRTEM experiments were performed on an FEI Talos 200X microscope operated at 200 kV. Nanoindentation tests were performed by using Hysitron TI Premiere. *In situ* micropillar compression tests were performed by using Hysitron PI 88xR PicoIndenter inside a FEI Quanta 3D FEG Dual-beam scanning electron microscopy (SEM) microscope. Cu/Co multilayer pillars with different layer thickness (5, 25 and 100 nm) were fabricated using Quanta 3D dual beam SEM microscope with the focused-ion-beam (FIB) set-up. The diameter of the pillars was ~1 μm. The height/diameter aspect ratio was kept at ~ 2:1 for the micropillars, following general consensus [36–38].

MD simulation compressions on cylindrical nanopillars of Cu/Co multilayers were performed using LAMMPS [39] to study the effect of extrinsic size effect and interface coherency on mechanical behaviors of Cu/Co multilayers. For the FCC Cu/HCP Co 10 nm pillar, it has similar structure with the nanopillar we studied in Part I [1] but with larger individual thickness of 10 nm, and the diameter is 15 nm. The Cu layers contain CTBs with a twin spacing of 3 nm, similar to the twin density in the single Cu layer in Cu/Co 25 nm experimental sample, and the Co layers contain SFs with a SF spacing of 1 nm. For the simulation of FCC Cu/FCC Co 5 nm pillar, the thickness of each layer is 5 nm, and the diameter is 15 nm. To control the variables, the CTBs spacing is set at 1.5 nm, keeping the same twin density with the simulated FCC Cu/HCP Co 10 nm pillar. The height of both pillars is 30 nm, keeping a height/diameter aspect ratio of 2:1. The crystallographic orientations of MD specimens are consistent with our experimental specimens. However, the individual layer thicknesses and overall dimensions for simulations are much smaller than those of the experimental specimens due to computational cost. Thus, we use FCC Cu/HCP Co 10 nm pillar to mimic mechanical behavior of Cu/Co 25 nm sample. To circumvent this size issue and to elucidate the atomistic underpinnings of the layer thickness dependent deformation mechanisms, the MD specimens are designed to show key differences between microstructures, including the nature of interface, namely FCC Cu/FCC Co and FCC Cu/HCP Co, and the presence of defect network in the FCC Cu/HCP Co specimen.

The simulations were performed at 300 K under the NVT canonical ensemble. The interactions between Cu and Co were modeled by the embedded-atom method (EAM) potential developed by Zhou et. al [8]. The potential was validated by calculating the elastic constants and the stacking fault energies for Cu as well as Co. The values were found to be in reasonable agreement with experimental results as well as simulation results performed using another EAM potential for HCP and FCC Co developed by Mishin et. al [40]. Non-periodic boundary conditions were used in all directions. First, conjugate gradient energy minimization was performed, followed by equilibration of the specimens at 300 K. Then, the specimens were subjected to compression at a constant strain rate of 1.86×10^8 s^{-1}. The HCP/FCC multilayer specimens were created layer by layer in order to introduce pre-existing CTBs in the FCC Cu layers and SFs in the Co layers parallel to the basal plane, to be consistent with the experimental specimens. The defect structures were visualized using OVITO [41].

3. Results

XRD patterns of Cu/Co multilayers with different layer thickness (Fig. 1a) reveal epitaxial growth of Cu (111) and Co (0002) when h = 25 and 100 nm. When h decreases to 5 nm, satellite peaks emerge, indicating the formation of coherent interface between Cu and Co. Fig. 1b shows the hardness of multilayers increases with decreasing h following the general 'smaller is stronger' trend. Fig. 2 shows cross-section TEM (XTEM) micrographs of Cu/Co multilayers examined from the Cu [110] zone axis. At lower magnification (Fig. 2a, d, h), the column size d of Cu/Co multilayers varies with different h. Average d is 57 and 48 nm respectively when h is 5 and 25nm, and increases to ~113 nm when h is 100nm (Statistics study is shown in supplementary Fig. S1). The formation of the FCC Cu and HCP Co phases is confirmed by selected area diffraction (SAD) pattern (Fig. 2a,d,g). Twin spots in FCC phase are also observed in the SAD patterns. When h = 5 and 25 nm, CTBs traverse the column and are arrested at column boundaries, forming perfect CTBs with litter incoherent twin boundary (ITB) steps. However, defective CTBs with ITB steps are observed in Cu/Co 100 nm multilayers (Fig. 2i). Parallel SFs on basal planes are also observed in Co layer (Fig. 2e, f, h). The Cu/Co interface is incoherent when h = 25 and 100 nm (Fig. 2e,h). However, when h decreases to 5 nm, coexistence of FCC Co and HCP Co is observed with similar fraction (Fig. 2b). FCC Co are mostly formed near the Cu layer, making the layer interface coherent between Cu and Co (Fig. 2c).

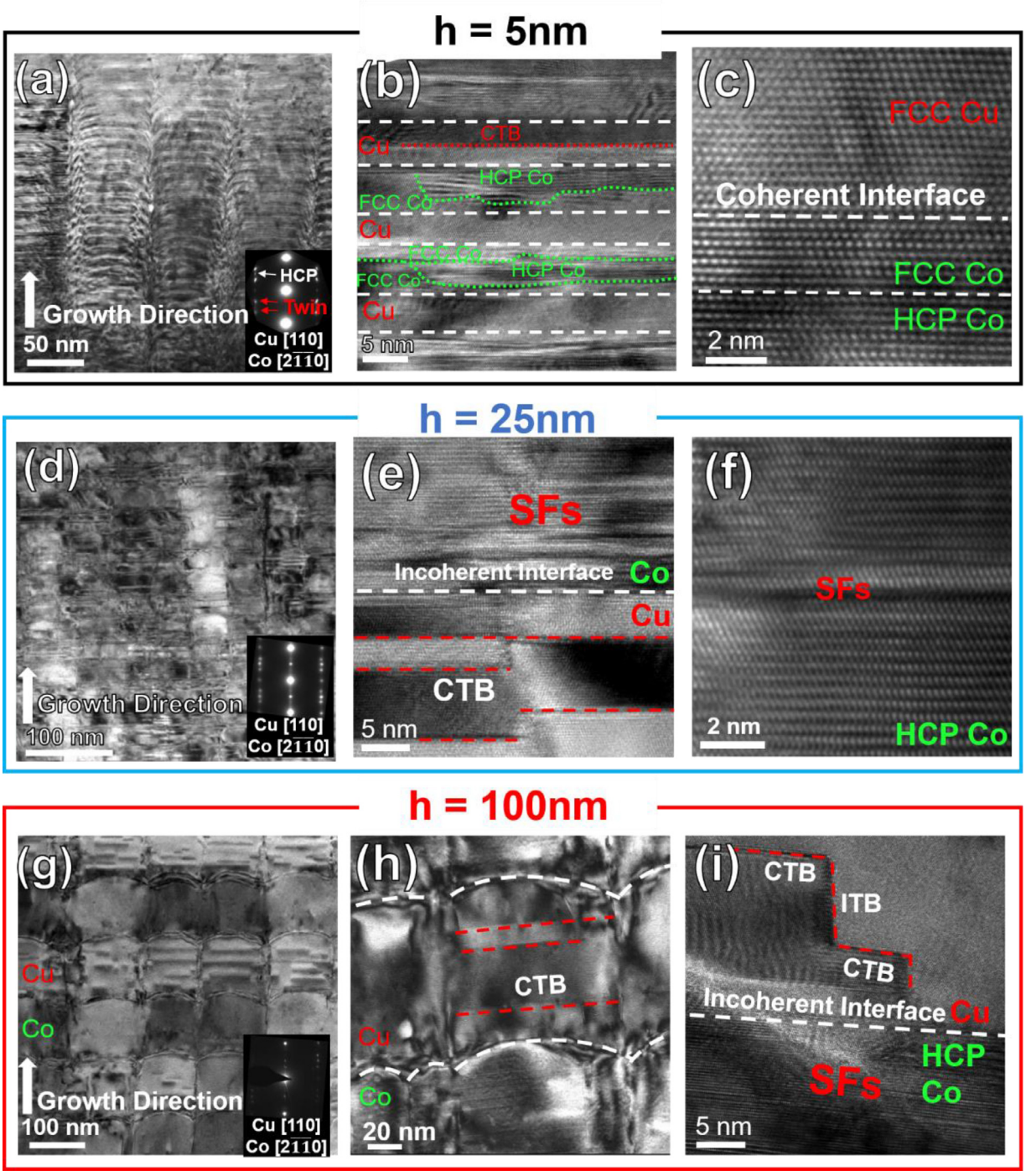

Fig. 2. Cross-section TEM (XTEM) micrographs of Cu/Co multilayers with individual layer thickness of 5, 25 and 100 nm. Selected area diffraction (SAD) patterns show FCC Cu and HCP Co phases in all three samples. (a) XTEM micrograph of the Cu/Co 5 nm multilayer examined from the Cu [110] zone axis showing that the average columnar grain size is 57 nm. (b) A higher magnification TEM micrograph showing column boundary and co-existence of FCC Co and HCP Co. Most Cu/Co interfaces become coherent. Twin boundaries are randomly distributed. (c) High resolution TEM (HRTEM) micrograph showing 2 nm thick FCC Co near the Cu/Co interface. (d) XTEM micrograph of the Cu/Co 25 nm multilayer examined from the Cu [110] zone axis. The average column size is 52 nm. (e) A higher magnification TEM micrograph showing high-density SFs in Co layer and CTBs in Cu layer. Twin spacing in Cu is 8 nm. The layer interface between Cu and Co is incoherent. (f) HRTEM micrograph of SFs in HCP Co. (g) XTEM micrograph of Cu/Co 100 nm multilayer from the Cu [110] zone axis. The average column size is 113 nm. (h) A higher magnification TEM micrograph showing CTBs in Cu layers. The average twin spacing is 30 nm. (i) HRTEM micrograph showing defective CTB with ITB steps in Cu layer and incoherent layer interface between Cu and HCP Co.

SFs are mostly observed in the HCP Co and TBs are randomly observed in several Cu layers (Fig. 2b). The curvature of interface in Cu/Co 5 nm is obviously larger than the other two multilayers due to larger residual stress at smaller layer thickness. But the residual stresses of three multilayers are a few hundred MPa or less, and have insignificant impact on the deformation behaviors of these high strength nanolayers. Also, the intensity of HCP spot in the SAD pattern of the Cu/Co 5 nm multilayer becomes weaker, indicating a larger fraction of FCC Co in Cu/Co 5 nm multilayer.

To investigate the mechanical behavior of Cu/Co multilayers with different *h*, systematic *in situ* SEM pillar compression tests were performed (Fig. 3). Due to the non-uniform deformation in

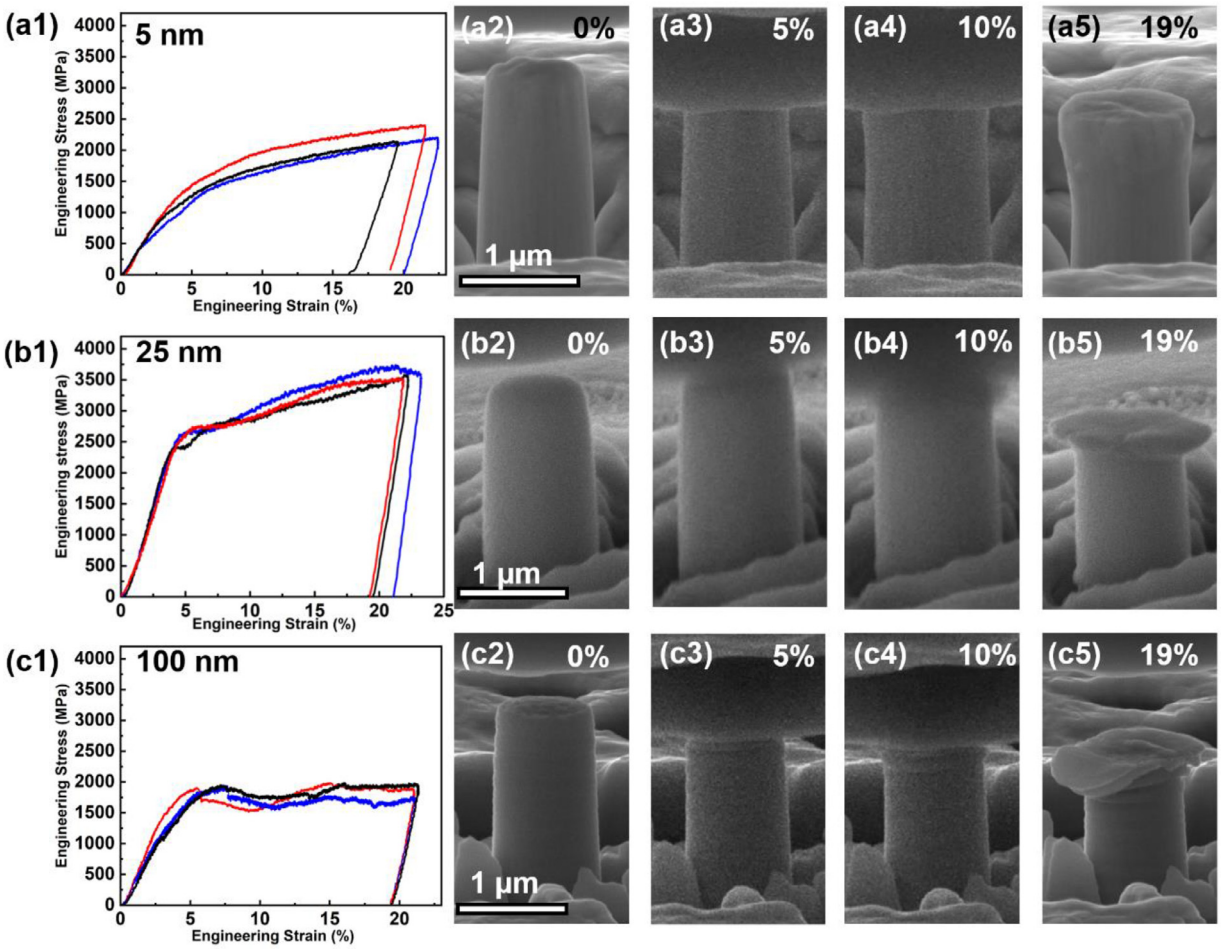

Fig. 3. (a1, b1, c1) Engineering stress-strain curves of Cu/Co multilayers with different *h*. The Cu/Co 25 nm multilayer has the highest flow stress. (a2-a5) SEM images of the Cu/Co 5 nm multilayer captured during *in situ* compression test show barreling at the top and a small shear band. (b2-b5) When $h = 25$ nm, significant plastic deformation was accumulated primarily at the top portion (~500 nm) of the pillar, forming a cap, while the bottom portion remained largely undeformed. (c2-c5) For the Cu/Co 100 nm multilayer, severe deformation took place mostly in the Cu layers, while Co layers remained rigid. See supplementary videos 1-3 for more details.

certain pillars, we plot the engineering stress-strain curves instead of true stress-strain curves to compare their mechanical properties. Cu/Co 5 nm pillars have an average yield strength of 1008 MPa and show prominent work hardening to an average flow stress of 1809 MPa at 10% engineering strain. The Cu/Co 25 nm pillars exhibit the highest average yield strength of 2486 MPa and flow stress of 3000 MPa (at 10% engineering strain) among the three specimens. The average yield strength and flow stress (at 10% engineering strain) of the Cu/Co 100 nm pillars is 1186 MPa and 1665 MPa, respectively. SEM snapshots of Cu/Co pillars recorded during compression tests reveal different morphology. When *h* is 5 nm, traditional barreling at the pillar top occurs, leading to the reverse conical shape (Fig. 3a5). A small shear band was also observed, to be shown later in TEM analysis. When $h = 25$ nm, plastic deformation is accumulated near the top layer (~500 nm), while the pillar base deforms only insignificantly. When $h = 100$ nm, there is little uniform co-deformation of the Cu and Co layers. Instead, a single layer yields first (Fig. 3c3) and multiple layers are extruded out (Fig. 3c4,c5), as reflected by the wavy stress-strain curves. These extruded layers are shown to be Cu layers by TEM analyses (Fig. 4) which will be discussed later in detail. The SEM snapshots of the three deformed pillars for each layer thickness are presented in supplementary Fig. S2 to show good reproducibility. *In situ* compression details are provided in supplementary video 1-3.

4. Discussion

The mechanical behaviors of the Cu/Co 25 nm multilayers were thoroughly investigated via both experiments and MD simulations and discussed in Part I of the study [1]. Its superior strength and deformability were attributed to defect networks of parallel planar interfaces, which consist of CTBs in Cu, SFs in Co and the incoherent layer interfaces.

In Part II, we will discuss the formation of these defect networks at different layer thickness *h* and their role in governing the mechanical properties of the Cu/Co multilayers.

4.1. Non-uniform deformation of Cu/Co 100 nm multilayers

XRD and TEM studies show that Cu/Co 100 nm multilayers have TBs in Cu layers, SFs in Co layers and incoherent layer interfaces (Fig. 1a, 2h), comprising the defect networks. However, instead of the Cu and Co co-deformation reported in the Cu/Co 25 nm multilayers [1], Cu/Co 100 nm multilayers show a non-uniform deformation after yielding, manifested by the preferential extrusion of Cu layers (Fig. 3c), due to the strength disparity between FCC Cu (111) and HCP Co (0002) layers. The preferential deformation of the softer layer is also observed in Cu/Zr, Cu/a-CuNb and Al/Pd multilayers [17,18,28,35]. HCP Co (0002) can hardly deform under compression because the resolved shear stresses on either basal

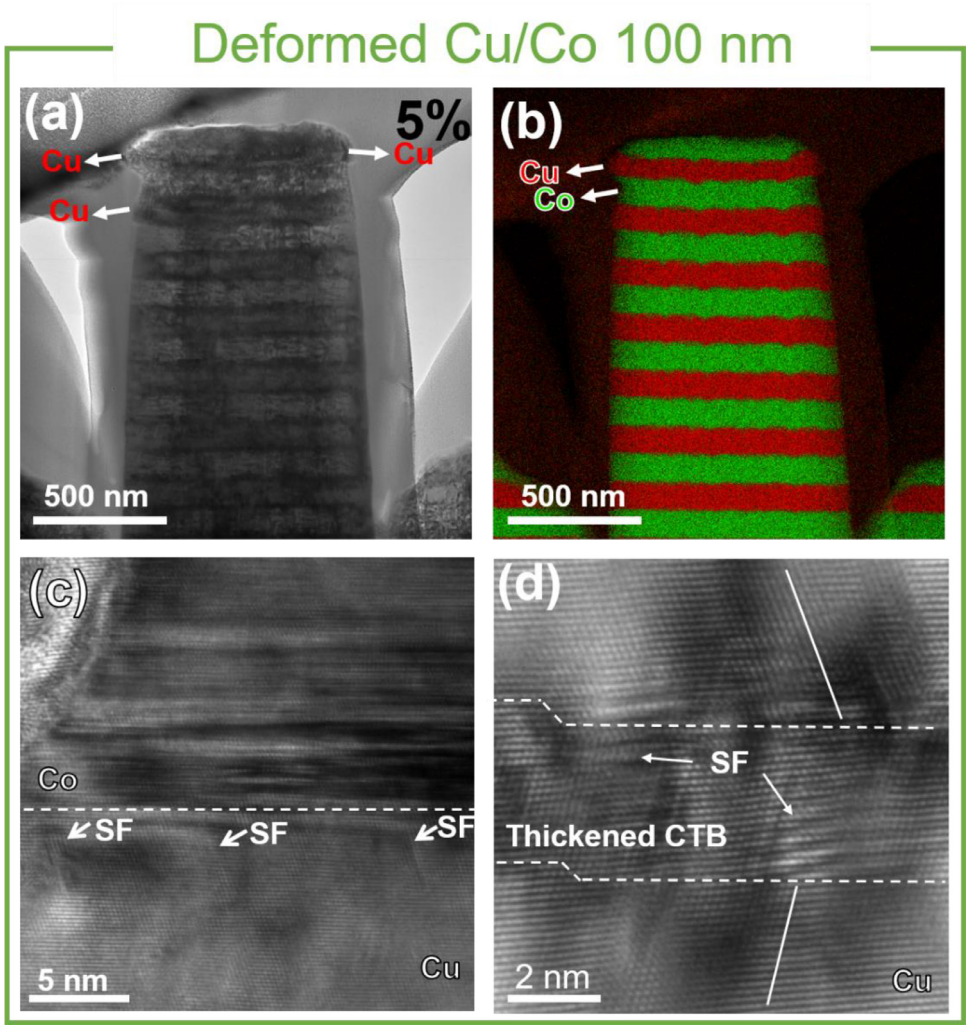

Fig. 4. (a) XTEM micrograph of Cu/Co 100 nm pillar deformed to 5% strain. (b) EDS map of the deformed Cu/Co 100 nm pillar showing extrusion of Cu layer at the onset of yielding. (c) TEM micrograph showing partial dislocations nucleating from Cu/Co interface and propagating into the Cu layer, leaving traces of SFs. (d) HRTEM micrograph showing detwinning in Cu layer. TBs were thickened and decorated with SFs and ITB steps.

planes or prismatic planes are negligible. Gliding of **c+a** type dislocations along pyramidal planes is also prohibited by high-density SFs (Fig. 2h) [42]. Therefore, in Cu/Co 100 nm pillars, HCP Co remains rigid during deformation. In contrast, the Cu layers are much softer than the Co layers, and thus substantial deformation accumulates in the Cu layers.

It is interesting to note that the Cu/Co 100 nm multilayers also contain defect networks. However, the deformation mechanism of this multilayer is quite different compared to the Cu/Co 25 nm multilayers. The Cu/Co 100 nm multilayer has much lower flow stress than that of the Cu/Co 25 nm multilayer. Although CTBs are also observed in the Cu layers in the Cu/Co 100 nm multilayer, the average twin spacing is 25 nm (supplementary Fig. S3), which is much larger than that in Cu/Co 25 nm multilayers (8 nm). Also, the ITBs in the Cu/Co 25 nm multilayers exist mostly in form of columnar grain boundaries locked by Cu/Co interfaces, and are less mobile. But ITBs in Cu/Co 100 nm multilayer are steps of CTBs, which are mobile and easy sources for detwinning (Fig. 2i). ITBs consist of mobile Shockley partials, which can trigger detwinning (supplementary Fig. S4) during deformation [43–47]. Additionally, the large layer thickness (100 nm) permits dislocation pile-ups along the inclined (relative to layer interface) slip planes during deformation. These differences in the microstructure lead to a much lower flow stress in the Cu/Co 100 nm multilayer than the Cu/Co 25 nm multilayer.

The preferential plastic deformation within the Cu layers derives from the strength disparity between Cu and Co in the Cu/Co 100 nm multilayers. Post deformation TEM and EDS analyses on Cu/Co 100 nm pillar show that Cu layers were squeezed after yielding while Co layers remained largely undeformed (Fig. 4a,b). Shockley partial dislocations nucleate from the Cu/Co interface and interact with CTBs (Fig. 4c). The interactions introduce ITB steps (Fig. 4d), which are known to be mobile [43–48] and the migration of ITBs leads to detwinning and softening. *In situ* compression of Cu/Co 100 nm pillar (supplementary video 1) shows that the stress drop corresponds to the preferential extrusion of the soft Cu layer. When the flat punch keeps compressing the pillar and approaches the hard Co layer, stress increases again (Fig. 3c1) until the next Cu layer starts to deform. Thus, the non-uniform deformation and the wavy stress-strain curve in Fig. 3c1 originates from the strength disparity between the FCC Cu and HCP Co layer. In contrast, in the Cu/Co 25 nm multilayer, Cu and Co layers with high-density CTBs and SFs co-deform, leading to uniform deformation, albeit localized in the pillar top [1].

When we studied the non-uniform deformation in pillar compression experiments, tapering is often an important factor, which

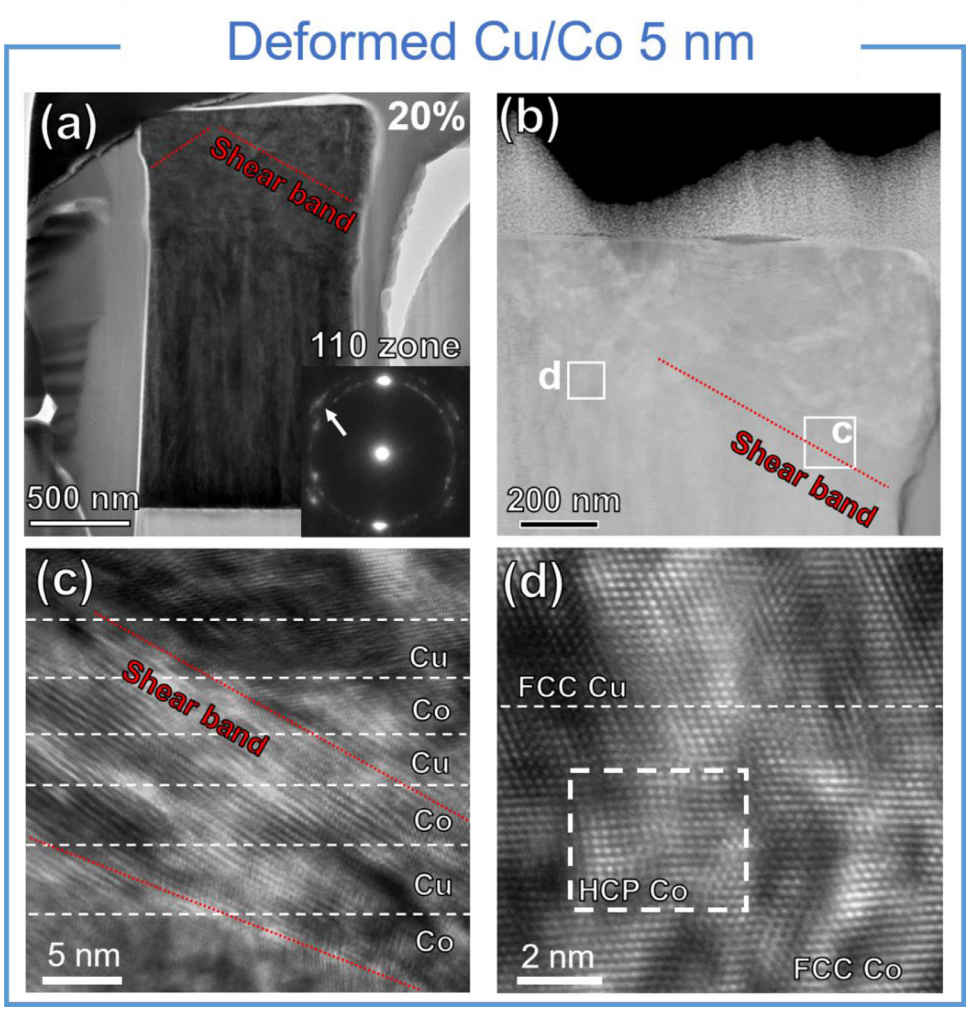

Fig. 5. XTEM micrographs and EDS maps of deformed Cu/Co 5 nm multilayer pillars. TEM (a) and STEM (b) micrographs of pillar deformed up to 20% strain showing dilation of the pillar top, and the generation of shear bands. (c) HRTEM micrograph showing abundant inclined SFs penetrating through Cu/Co layer interface. (d) HRTEM micrograph showing the formation of primarily FCC Co with little HCP Co patches.

leads to a higher local stress at the top part of the pillar. But in both Part I and this study [1], we have fine-tuned the FIB parameter to minimize the tapering and control the taper angle of all pillars to a similar value in order to eliminate the effect of tapering on mechanical behaviors. Only the FCC Cu/HCP Co 25 nm and 100 nm samples show severely deformed cap layers. The former one is due to detwinning and phase transformation induced co-deformation of Cu/Co layers, which have been investigated in Part I of the story [1]. The latter one is due to the extrusion of soft Cu layers. Other pillars with the same aspect ratio and taper angle do not have such non-uniform deformation (Supplementary Fig. S5). Thus, we rule out the influence of the pillar geometry when studying the mechanical behaviors of Cu/Co multilayers.

4.2. Interface dominated softening in coherent Cu/Co 5 nm multilayers

In contrast to 'smaller is stronger', Cu/Co 5 nm pillars have an average flow stress of 1809 MPa (when $\varepsilon = 10\%$) under compression, much less than the Cu/Co 25 nm pillars with an average flow stress of 3000 MPa at a similar strain level. There are several microstructural differences between the two sets of multilayers. First, the Cu/Co 5 nm multilayer has significantly fewer CTBs and SFs than the Cu/Co 25 nm multilayer. Second, the Cu/Co 5 nm multilayer has a coherent layer interface. FCC Co grows on top of Cu (111) due to a small lattice mismatch strain, 2.3% (a_{Cu} = 3.615 Å, a_{Co} = 3.548 Å) [3], thereby forming a coherent FCC Cu/ FCC Co interface, as revealed by XRD (Fig. 1a) and HRTEM micrograph (Fig. 2c). The lack of defect network in the Cu/Co 5 nm multilayer thus leads to a lower flow stress than that of the Cu/Co 25 nm multilayer.

To investigate the deformation mechanisms in Cu/Co 5 nm pillars, post deformation TEM analysis is performed as shown in Fig. 5. The ring shape in SAD (Fig. 5a) indicates layer rotation. A shear band is observed in XTEM (Fig. 5a) and STEM (Fig. 5b) micrographs. Near the shear band region (Fig. 5c), high-density inclined SFs and slip traces are observed, resulting from the transmission of Shockley partial dislocations across the Cu/Co interface along inclined (111) planes. HRTEM micrograph in Fig. 5d shows a majority of the Co layer has FCC phase with scattered HCP Co patches.

In metallic multilayers, when h is less than 10 nm, the transmission of single dislocations across layer interface is the dominant deformation mechanism [5,7,10,13,14,49,50]. Under compression, partial dislocations gliding along inclined (111) planes can easily propagate across the coherent Cu (111)/Co (111) interface, significantly degrading the strength of the Cu/Co 5 nm multilayer.

In Part I of the study [1], MD simulations of compression of Cu/Co multilayer pillars with incoherent interface were per-

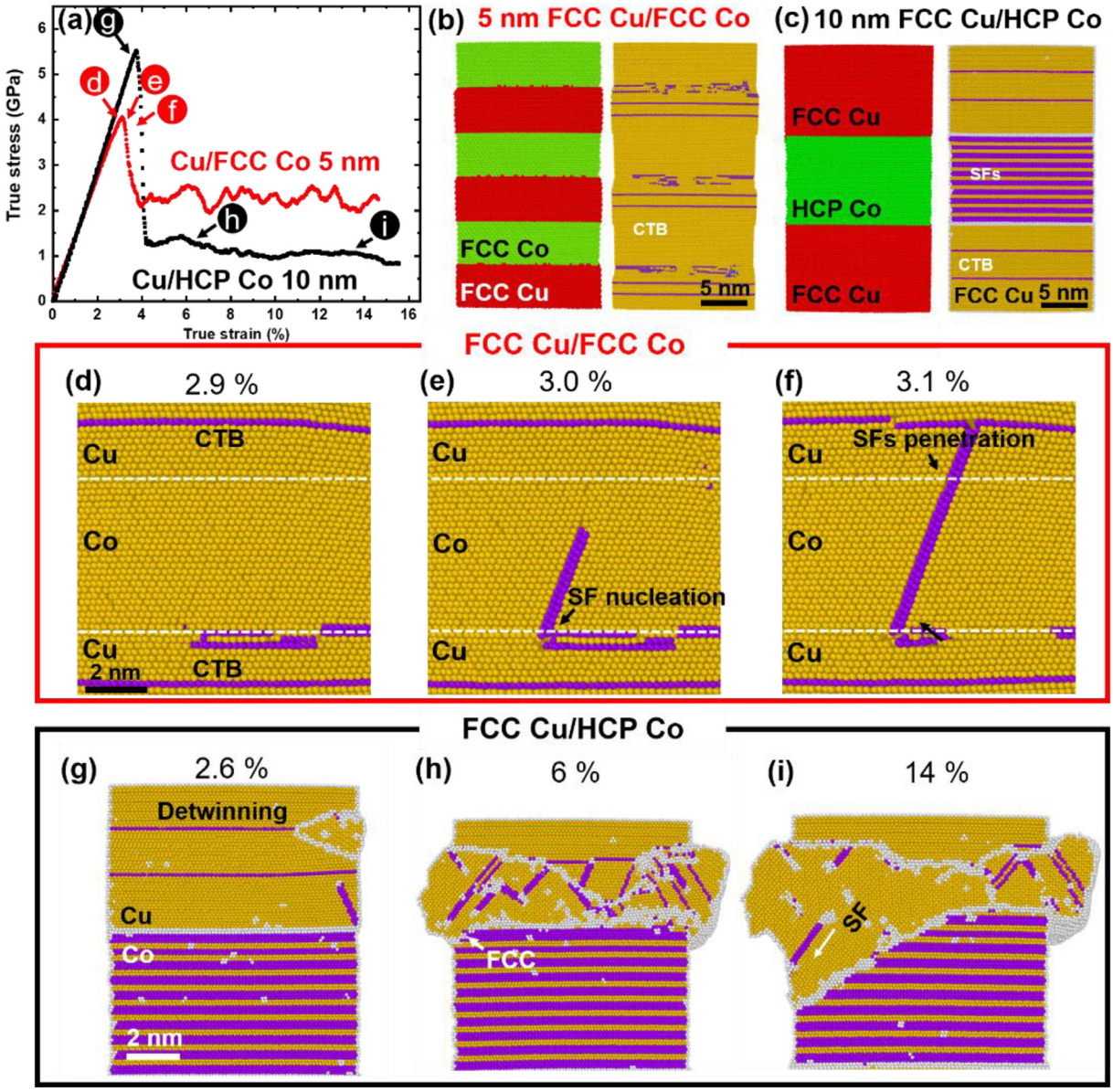

Fig. 6. MD simulation of compression of FCC Cu/FCC Co 5 nm and FCC Cu/HCP Co 10 nm multilayer pillars. (a) Stress-strain curves for the two Cu/Co nanopillars. FCC Cu/HCP Co 10 nm multilayer yields at ~6 GPa, while FCC Cu/FCC Co 5 nm specimen has a lower yield strength, ~4 GPa. (b,c) Structures of FCC Cu/FCC Co 5 nm with coherent layer interface and CTBs in Cu layers, and FCC Cu/HCP Co 10 nm multilayer with defect network consisting of CTBs in Cu, SFs in HCP Co, and incoherent layer interface. Left panel shows Cu in red and Co in green. Right panel shows atoms in FCC (yellow) and HCP (purple) structure in common neighbor color coding. (d-f) Microstructural evolution and dislocation activity in FCC Cu/FCC Co pillar. (d) Before yielding, parallel SFs are observed at the Cu/Co interface. (e) Inclined SFs nucleate at the Cu/Co interface. (f) Inclined SFs transmit across the coherent Cu/Co interface and lead to the stress drop. (g-i) Microstructural evolution and dislocation activity in FCC Cu/HCP Co pillar. (g) Detwinning occurs in Cu layer before yielding. (h) HCP-to-FCC Co phase transformation occurs at the Cu/Co interface. (i) When Co transforms to FCC structure, the interface between Cu and Co becomes coherent. SFs can now easily transmit through the coherent interface, leading to softening. See supplementary videos 4-7 for more details.

formed to elucidate the atomistic underpinnings of the collaborative strengthening effect of defect networks (see details in supplementary Fig. S6). Those simulations revealed that dislocations cannot transmit through the incoherent layer interface due to slip discontinuity between FCC (111) and HCP (0002) [1]. Abnormal softening in 5 nm multilayers could come from the coherent layer interface. To investigate the different role of incoherent and coherent interfaces on blocking dislocations, we present two new MD simulations to systematically examine the effect of interface coherency on dislocation activity and mechanical behaviors of Cu/Co multilayers (Fig. 6). Fig. 6b and Fig. 6c show the microstructure of a FCC Cu/FCC Co 5 nm multilayer nanopillar with a coherent interface and an FCC Cu/HCP Co 10 nm nanopillar with an incoherent interface (Complete compression simulations with structural evolution and dislocation activity are provided in supplementary videos 4-7). True stress-strain curves (Fig. 6a) show that the FCC Cu/FCC Co 5 nm pillar has a much lower yield strength (~4 GPa) than that of FCC Cu/HCP Co 10 nm pillar (~ 5.5 GPa). In the case of FCC Cu/FCC Co 5 nm pillar, at the onset of yielding (Fig. 6d-f), Shockley partials are transmitted across the coherent Cu/Co interface as signaled by SF penetration and a dramatic stress drop after 3.2% strain. In contrast, in the case of FCC Cu/HCP Co 10 nm pillar, partial dislocations cannot transmit through the incoherent FCC Cu/HCP Co interface (Fig. 6g). Instead, HCP-to-FCC Co phase transformation is triggered to accommodate the plastic deformation, similar to the MD simulations for the FCC Cu/HCP Co 5 nm pillar described in Part I [1]. SFs can propagate into the Co layer after it is transformed to the FCC phase (Fig. 6i).

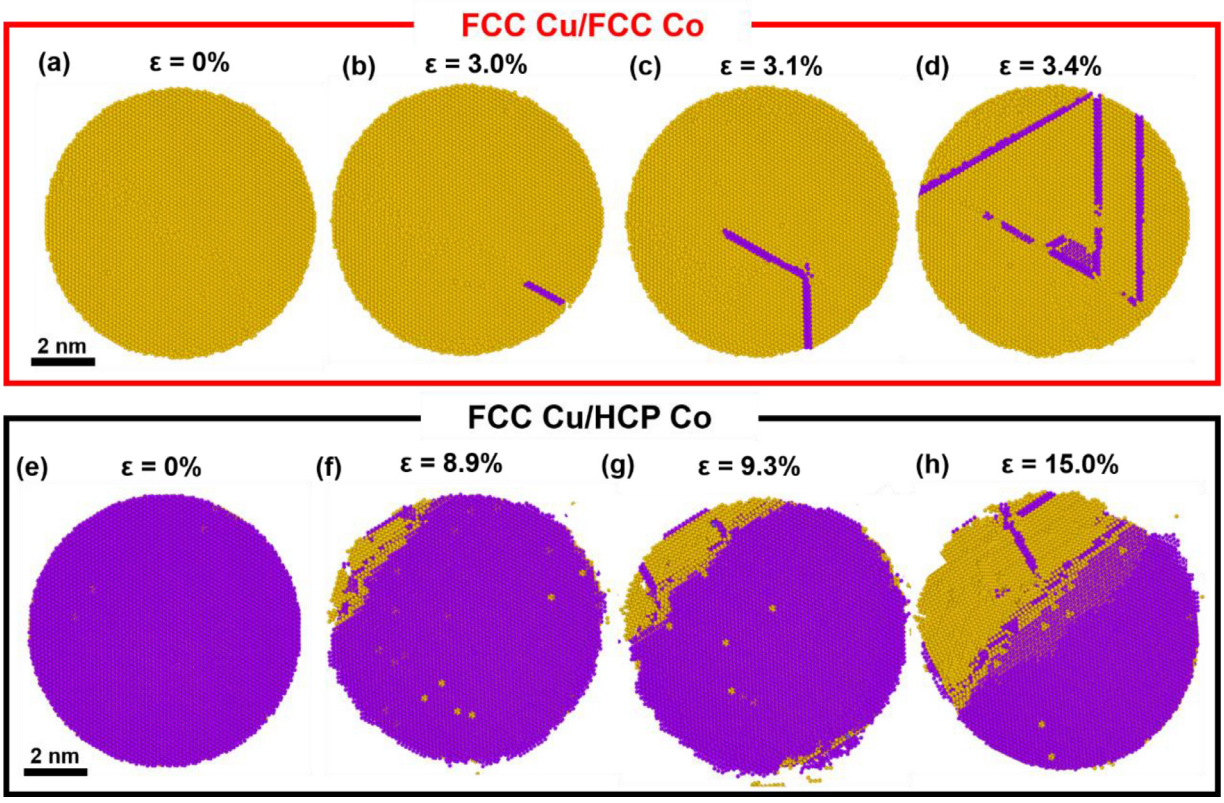

Fig. 7. Top view of the layer interface in (a-d) FCC Cu/FCC Co 5 nm nanopillar and (e-h) FCC Cu/HCP Co 10 nm nanopillar at different strain levels. Atoms are in common neighbor color coding, where orange denotes FCC and purple denotes HCP. (a) FCC/FCC coherent interface before yielding. (b) When $\varepsilon = 3.0\%$, SFs begin to nucleate at the interface. (c-d) After yielding, multiple SFs penetrate through the interface. (e) Before compression, the incoherent interface has HCP Co phase. (b) When $\varepsilon = 3.9$ %, HCP Co begins to transform to FCC phase initiating from the pillar surface. (g) As more FCC Co phase is formed, inclined SFs emerge inside the FCC phase. (h) More than half of HCP Co is transformed to FCC Co and abundant inclined SFs are observed across the interface.

The difference in the nature of the interface - incoherent versus coherent - is clearly revealed in the top-down view of MD snapshots shown in Fig. 7. In the FCC Cu/FCC Co 5 nm pillar, SFs penetrate the coherent interface at yield point (Fig. 7b). As strain increases, more SF penetration is observed. Coherent FCC (111) interface is a weak barrier to the transmission of partial dislocations (dislocation evolution is shown in supplementary Figure S7 and supplementary video 5). Similar phenomenon has been observed in (100) and (110) textured FCC Cu/Co multilayers with coherent interfaces as discussed in Part I [1]. However, during deformation of the FCC Cu/HCP Co nanopillar, the incoherent interface gradually transforms into a coherent interface as HCP Co is transformed to FCC phase. SFs can then penetrate through the coherent interface as shown in Fig. 7g,h.

MD simulations reveal the details of partial dislocation and SF penetration process based on the different nature of interfaces, which are in good agreement with our experimental results. MD studies also reveal that the defect network requires all three planar defects (TBs, SFs, incoherent interfaces) to work together in order to provide optimum strengthening effect.

5. Strength discrepancy in Cu/Co 25 nm multilayers between compression and nanoindentation

The ultra-high strength and deformability of Cu/Co 25 nm multilayers have been reported in Part I [1]. CTBs in Cu, SFs in Co and incoherent layer interfaces form collaborative defect networks, which inhibit the glide of dislocations in both Cu and Co layers, and hinder the transmission of dislocations across the interfaces, enabling the extraordinary strength of Cu/Co 25 nm pillar under compression. In contrast, the lower strength observed in Cu/Co 100 nm indicates that, in addition to the defect network, defect density is also critical in achieving high strength. The CTB and SF spacing in Cu/Co 25 nm multilayers are 8 nm and 5 nm respectively. Whereas, the Cu/Co 100 nm multilayer has an average twin spac-

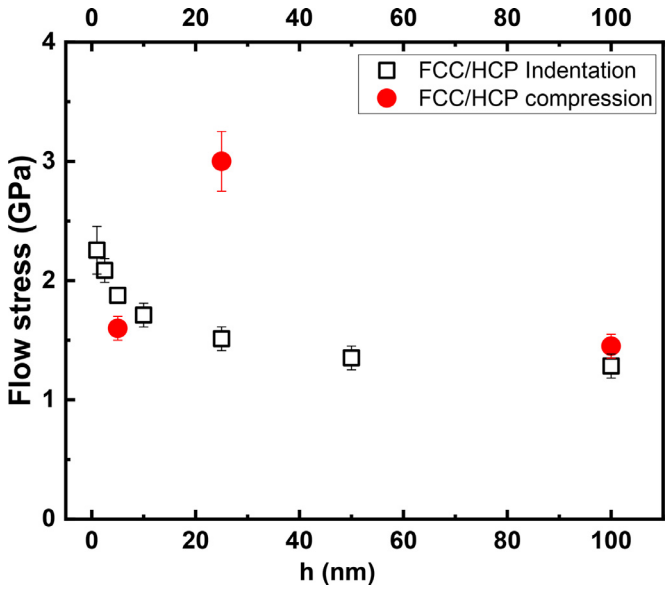

Fig. 8. Comparison of flow stress calculated from nanoindentation measurements (flow stress = hardness/2.7) with those obtained from *in situ* micropillar compression tests (at a strain of 10%) for the same sets of Cu/Co multilayers.

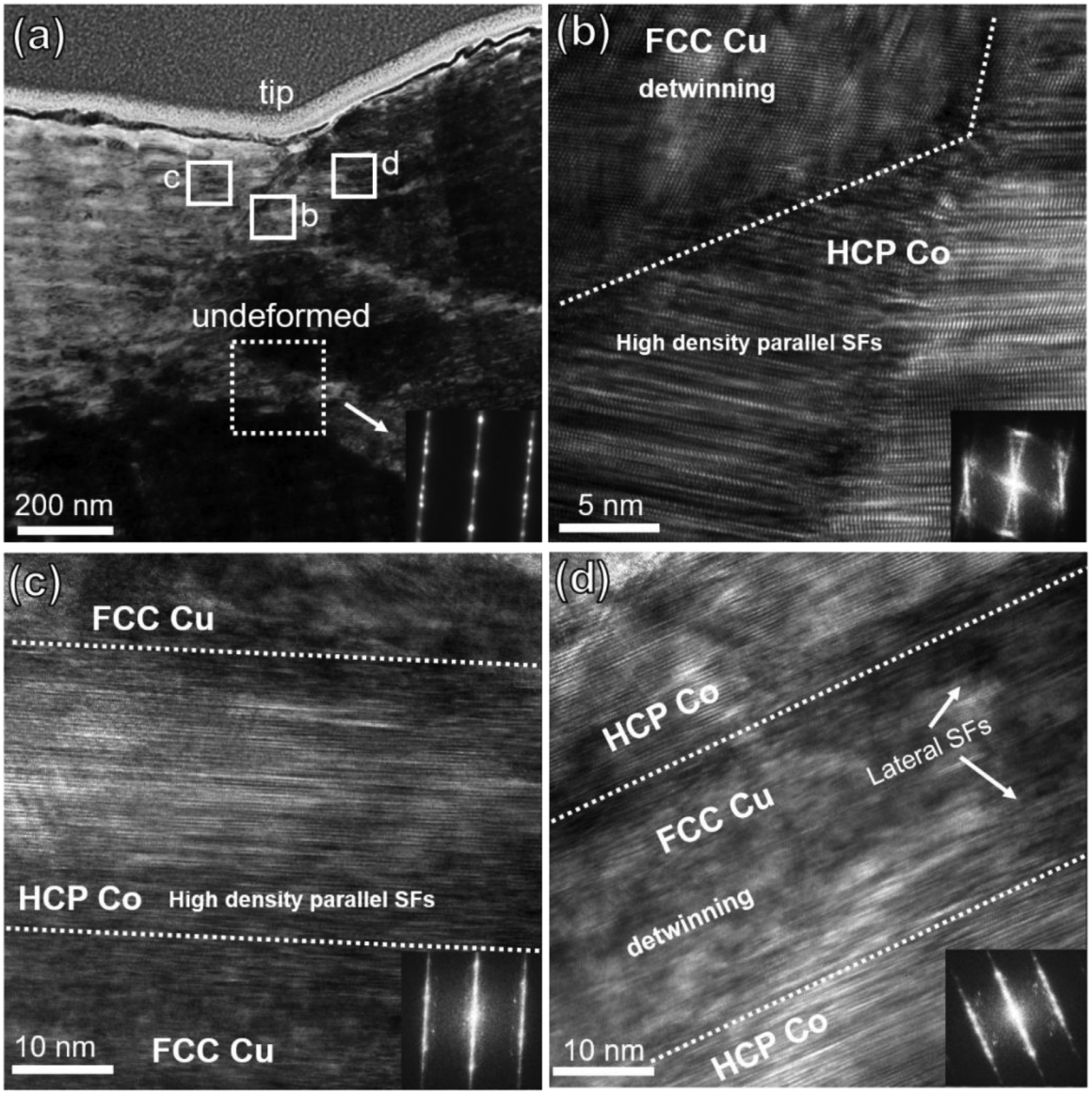

Fig. 9. (a) XTEM micrograph of Cu/Co 25 nm multilayer after 200 nm nano-indentation. (b) Deformed region underneath the indent. High density SFs are observed in HCP Co. Detwinning occurred in Cu layer and twin boundary is rarely observed. (c,d) left and right region near the indent. High density lateral SFs are formed in both Cu and Co layer. Twin boundaries in Cu layer and phase transformation in Co layer are not observed.

ing of 25 nm in Cu (supplementary Fig. S3) and significantly fewer SFs in HCP Co.

Hardness of Cu/Co multilayers has been studied before [3]. In this study, we also use nanoindentation to measure the hardness of Cu/Co multilayers and the results are reproducible. To investigate the relationship of strength in Cu/Co multilayers under nanoindentation and compression, hardness measured by nanoindentation is converted to flow stress by dividing by the Tabor factor (2.7) [51] and compared with the flow stress measured by pillar compression (Fig. 8). For the Cu/Co 5 nm and 100 nm multilayers, the flow stresses measured by micropillar compression tests are consistent with the converted flow stresses measured by nanoindentation. However, the Cu/Co 25 nm multilayers have much higher flow stress (~3 GPa) under compression, which is two times larger than the flow stress obtained from nanoindentation. This large discrepancy between indentation strength and compression strength in Cu/Co 25 nm multilayers is due to different deformation modes of Cu/Co 25 nm under indentation and compression. Deformation mechanism in metallic multilayers is layer thickness dependent. In the Cu/Co 100 nm multilayers, the major deformation mechanism is the glide of partial dislocations along inclined (111) planes in the Cu layer, leading to detwinning and Cu extrusion. In the Cu/Co 5 nm multilayers, the dominant deformation mode is the transmission of a single dislocation through the coherent layer interface along the inclined (111) plane. The common feature of both samples is that the resolved shear stress along inclined (111) planes determines the dislocation activity. The different stress field between nanoindentation and pillar compression does not lead to different deformation mode in the Cu/Co 100 nm and 5 nm samples because dislocations gliding along inclined (111) planes dominates in both indentation and compression tests in these two systems.

However, it is well known that when h is between 5-50 nm, CLS is the dominant deformation mechanism in the Cu/Co 25 nm multilayers where dislocations prefer to glide laterally in between the layer interfaces [2,5,7,13,15,21,33,35,52,53]. The defect network in Cu/Co 25 nm multilayers also has a unique characteristic, that is the three types of defects (TBs, interfaces and SFs) are all parallel to each other. Such a unique geometry may lead to

the large anisotropic behavior. Under compression, resolved shear stress along lateral direction is nearly zero, which hinders CLS. Also, the glide of dislocations along the inclined slip planes is difficult due to the existence of defect networks. High stress is needed to trigger the HCP-to-FCC Co phase transformation, leading to high strength in the Cu/Co 25 nm multilayers under compression. After yielding, the phase transformation converts incoherent layer interface into coherent interface, thus enables dislocation glide along inclined (111) planes [1]. However, when the Cu/Co 25 nm multilayer is subjected to nanoindentation, the dominant deformation mechanism is the glide of dislocations along lateral (111) planes in Cu and (0002) planes in Co. TEM analysis on the Cu/Co 25 nm multilayer after indentation to a depth of 200 nm is shown in Fig. 9. The SAD pattern taken from undeformed region is the same as the as-deposited sample, which has FCC Cu/HCP Co microstructure with high-density twins in Cu layers. TEM image underneath the indent (Fig. 9b) shows that high-density SFs were formed in HCP Co and FCC Cu, which is also confirmed by the streaking lines in the SAD pattern. Interestingly, there was little phase transformation induced FCC Co and detwinning was observed in the Cu layer. Fig. 9c and 9d taken from the left and right side of the indent show similar phenomena: high-density lateral SFs are formed in both FCC Cu and HCP Co layers. Twin boundaries were rarely observed in Cu layers and FCC Co was not observed. These observations validate our hypothesis that shear stress along lateral direction is much greater when Cu/Co multilayer undergoes nanoindentation than subjected to micropillar compression. CTBs and SFs do not arrest dislocation migration effectively in this case. The plastic deformation of Cu/Co 25 nm under indentation is mainly accommodated by partial dislocation migration along lateral (111) planes in FCC Cu, which leads to detwinning and the formation of SFs in Cu and HCP Co. The stress needed to move the dislocation is much lower than that necessary to trigger phase transformation. Thus, the converted flow stress of Cu/Co 25 nm under indentation is much less than under compression, and phase transformation would not occur.

6. Conclusion

We report drastically different deformation behavior of Cu/Co multilayers with same crystallographic orientation but different layer thickness. *In situ* micropillar compression studies show that Cu/Co 25 nm multilayer has the highest strength and best deformability. In the Cu/Co 100 nm multilayer, non-uniform deformation manifested by preferential Cu extrusion is observed due to dislocation pile-ups in Cu layer and detwinning induced softening. The Cu/Co 5 nm pillars are much softer than the Cu/Co 25 nm pillars due to the formation of coherent Cu/Co layer interfaces. MD simulations reveal that the transparent FCC Cu/Co interfaces are weak barriers to the transmission of dislocations. Strengthening imparted by defect networks requires the interplay of TBs, SFs and parallel incoherent layer interfaces as well as high defect density.

Declaration of Competing Interest

The authors declare that they have no known competing financial interests or personal relationships that could have appeared to influence the work reported in this paper.

Acknowledgement

RS and XZ acknowledge the financial support by NSF-DMR 1642759. DN and YK acknowledge the financial support by NSF-DMR 1508484. Pillar compression and TEM analysis by SX and QL are supported by DOE-OBES under grant No. DE-SC0016337. H. Wang acknowledges the support from the U.S. Office of Naval Research (N00014-17-1-2087). Accesses to the Life Sciences Microscopy Center and Materials Science Microscopy Center at Purdue University are also acknowledged. The support from the Research Computing Data Core at the University of Houston is also acknowledged. We also acknowledge access to facilities at DOE Center for Integrated Nanotechnologies.

Supplementary materials

Supplementary material associated with this article can be found, in the online version, at doi:10.1016/j.actamat.2020.116494.

Reference

[1] R. Su, D. Neffati, Q. Li, S. Xue, J. Cho, J. Li, J. Ding, Y. Zhang, C. Fan, H. Wang, Y. Kulkarni, X. Zhang, Ultra-high strength and plasticity mediated by partial dislocations and defect networks: Part I: Texture effect, Acta Materialia (2019).
[2] J. Li, Y. Chen, S. Xue, H. Wang, X. Zhang, Comparison of size dependent strengthening mechanisms in Ag/Fe and Ag/Ni multilayers, Acta Materialia 114 (2016) 154–163.
[3] Y. Liu, Y. Chen, K. Yu, H. Wang, J. Chen, X. Zhang, Stacking fault and partial dislocation dominated strengthening mechanisms in highly textured Cu/Co multilayers, International Journal of Plasticity 49 (2013) 152–163.
[4] I. Knorr, N.M. Cordero, E.T. Lilleodden, C.A. Volkert, Mechanical behavior of nanoscale Cu/PdSi multilayers, Acta Materialia 61 (13) (2013) 4984–4995.
[5] D. Bufford, Z. Bi, Q.X. Jia, H. Wang, X. Zhang, Nanotwins and stacking faults in high-strength epitaxial Ag/Al multilayer films, Applied Physics Letters 101 (22) (2012).
[6] J. Wang, A. Misra, An overview of interface-dominated deformation mechanisms in metallic multilayers, Current Opinion in Solid State and Materials Science 15 (1) (2011) 20–28.
[7] J.Y. Zhang, X. Zhang, R.H. Wang, S.Y. Lei, P. Zhang, J.J. Niu, G. Liu, G.J. Zhang, J. Sun, Length-scale-dependent deformation and fracture behavior of Cu/X (X=Nb, Zr) multilayers: The constraining effects of the ductile phase on the brittle phase, Acta Materialia 59 (19) (2011) 7368–7379.
[8] X.W. Zhou, R.A. Johnson, H.N.G. Wadley, Misfit-energy-increasing dislocations in vapor-deposited CoFe/NiFe multilayers, Physical Review B 69 (14) (2004) 144113.
[9] J. Wang, R.G. Hoagland, J.P. Hirth, A. Misra, Atomistic simulations of the shear strength and sliding mechanisms of copper-niobium interfaces, Acta Materialia 56 (13) (2008) 3109–3119.
[10] N.A. Mara, D. Bhattacharyya, P. Dickerson, R.G. Hoagland, A. Misra, Deformability of ultrahigh strength 5 nm Cu/Nb nanolayered composites, Applied Physics Letters 92 (23) (2008).
[11] A. Misra, X. Zhang, D. Hammon, R.G. Hoagland, Work hardening in rolled nanolayered metallic composites, Acta Materialia 53 (1) (2005) 221–226.
[12] A. Misra, M. Verdier, Y. Lu, H. Kung, T. Mitchell, M. Nastasi, J. Embury, Structure and mechanical properties of Cu-X (X= Nb, Cr, Ni) nanolayered composites, Scripta Materialia 39 (4) (1998) 555–560.
[13] Y. Liu, D. Bufford, H. Wang, C. Sun, X. Zhang, Mechanical properties of highly textured Cu/Ni multilayers, Acta Materialia (2011).
[14] J. McKeown, A. Misra, H. Kung, R.G. Hoagland, M. Nastasi, Microstructures and strength of nanoscale Cu–Ag multilayers, Scripta Materialia 46 (8) (2002) 593–598.
[15] Y. Chen, Y. Liu, C. Sun, K.Y. Yu, M. Song, H. Wang, X. Zhang, Microstructure and strengthening mechanisms in Cu/Fe multilayers, Acta Materialia 60 (18) (2012) 6312–6321.
[16] X. Zhang, A. Misra, H. Wang, T. Shen, M. Nastasi, T. Mitchell, J. Hirth, R. Hoagland, J. Embury, Enhanced hardening in Cu/330 stainless steel multilayers by nanoscale twinning, Acta materialia 52 (4) (2004) 995–1002.
[17] P. Dayal, M.Z. Quadir, C. Kong, N. Savvides, M. Hoffman, Transition from dislocation controlled plasticity to grain boundary mediated shear in nanolayered aluminum/palladium thin films, Thin Solid Films 519 (10) (2011) 3213–3220.
[18] W. Guo, E. Jägle, J. Yao, V. Maier, S. Korte-Kerzel, J.M. Schneider, D. Raabe, Intrinsic and extrinsic size effects in the deformation of amorphous CuZr/nanocrystalline Cu nanolaminates, Acta Materialia 80 (Supplement C) (2014) 94–106.
[19] J.Y. Zhang, J. Li, X.Q. Liang, G. Liu, J. Sun, Achieving optimum mechanical performance in metallic nanolayered Cu/X (X = Zr, Cr) micropillars, Scientific Reports 4 (2014) 4205.
[20] Y.Y. Lu, R. Kotoka, J.P. Ligda, B.B. Cao, S.N. Yarmolenko, B.E. Schuster, Q. Wei, The microstructure and mechanical behavior of Mg/Ti multilayers as a function of individual layer thickness, Acta Materialia 63 (2014) 216–231.
[21] B. Ham, X. Zhang, High strength Mg/Nb nanolayer composites, Materials Science And Engineering a-Structural Materials Properties Microstructure And Processing 528 (4-5) (2011) 2028–2033.
[22] S. Pathak, N. Velisavljevic, J.K. Baldwin, M. Jain, S. Zheng, N.A. Mara, I.J. Beyerlein, Strong, Ductile, and Thermally Stable bcc-Mg Nanolaminates, Scientific Reports 7(1) (2017) 8264.
[23] D. Bhattacharyya, N.A. Mara, P. Dickerson, R.G. Hoagland, A. Misra, Compressive flow behavior of Al-TiN multilayers at nanometer scale layer thickness, Acta Materialia 59 (10) (2011) 3804–3816.

[24] S.M. Han, M.A. Phillips, W.D. Nix, Study of strain softening behavior of Al-Al3Sc multilayers using microcompression testing, Acta Materialia 57 (15) (2009) 4473–4490.
[25] C.R. Mayer, L.W. Yang, S.S. Singh, J. Llorca, J.M. Molina-Aldareguia, Y.L. Shen, N. Chawla, Anisotropy, size, and aspect ratio effects on micropillar compression of AlSiC nanolaminate composites, Acta Materialia 114 (2016) 25–32.
[26] J.Y. Zhang, G. Liu, J. Sun, Self-toughening crystalline Cu/amorphous Cu–Zr nanolaminates: Deformation-induced devitrification, Acta Materialia 66 (2014) 22–31.
[27] Z. Fan, S. Xue, J. Wang, K.Y. Yu, H. Wang, X. Zhang, Unusual size dependent strengthening mechanisms of Cu/amorphous CuNb multilayers, Acta Materialia 120 (2016) 327–336.
[28] Z. Fan, Q. Li, J. Li, S. Xue, H. Wang, X. Zhang, Tailoring plasticity of metallic glasses via interfaces in Cu/amorphous CuNb laminates, Journal of Materials Research 32 (14) (2017) 2680–2689.
[29] Y. Kim, A.S. Budiman, J.K. Baldwin, N.A. Mara, A. Misra, S.M. Han, Microcompression study of Al-Nb nanoscale multilayers, Journal Of Materials Research 27 (3) (2012) 592–598.
[30] J.M. Wheeler, R. Raghavan, V. Chawla, J. Zechner, I. Utke, J. Michler, Failure mechanisms in metal–metal nanolaminates at elevated temperatures: Microcompression of Cu–W multilayers, Scripta Materialia 98 (2015) 28–31.
[31] N. Li, M. Demkowicz, N. Mara, Y. Wang, A. Misra, Hardening due to Interfacial He Bubbles in Nanolayered Composites, Materials Research Letters 4 (2) (2016) 75–82.
[32] Y. Cui, B. Derby, N. Li, N.A. Mara, A. Misra, Suppression of shear banding in high-strength Cu/Mo nanocomposites with hierarchical bicontinuous intertwined structures, Materials Research Letters 6 (3) (2018) 184–190.
[33] E. Fu, N. Li, A. Misra, R. Hoagland, H. Wang, X. Zhang, Mechanical properties of sputtered Cu/V and Al/Nb multilayer films, Materials Science and Engineering: A 493 (1) (2008) 283–287.
[34] A. Misra, J.P. Hirth, R.G. Hoagland, Length-scale-dependent deformation mechanisms in incoherent metallic multilayered composites, Acta Materialia 53 (18) (2005) 4817–4824.
[35] J.Y. Zhang, S. Lei, Y. Liu, J.J. Niu, Y. Chen, G. Liu, X. Zhang, J. Sun, Length scale-dependent deformation behavior of nanolayered Cu/Zr micropillars, Acta Materialia 60 (4) (2012) 1610–1622.
[36] M. Kuroda, Higher-order gradient effects in micropillar compression, Acta Materialia 61 (7) (2013) 2283–2297.
[37] I.-s. Choi, Y. Gan, D. Kaufmann, O. Kraft, R. Schwaiger, Measurement of Young's modulus of anisotropic materials using microcompression testing, Journal of Materials Research 27 (21) (2012) 2752–2759.
[38] H. Zhang, B.E. Schuster, Q. Wei, K.T. Ramesh, The design of accurate micro–compression experiments, Scripta Materialia 54 (2) (2006) 181–186.
[39] S. Plimpton, Fast Parallel Algorithms for Short-Range Molecular Dynamics, Journal of Computational Physics 117 (1) (1995) 1–19.
[40] G.P. Pun, Y. Mishin, Embedded-atom potential for hcp and fcc cobalt, Physical Review B 86 (13) (2012) 134116.
[41] A. Stukowski, Visualization and analysis of atomistic simulation data with OVITO–the Open Visualization Tool, Modelling and Simulation in Materials Science and Engineering 18 (1) (2010) 015012.
[42] R. Su, D. Neffati, J. Cho, Q. Li, J. Ding, H. Wang, Y. Kulkarni, X. Zhang, Phase transformation induced plasticity in high-strength hexagonal close packed Co with stacking faults, Scripta Materialia 173 (2019) 32–36.
[43] N. Lu, K. Du, L. Lu, H.Q. Ye, Motion of 1/3 < 111 >dislocations on Sigma 3 {112} twin boundaries in nanotwinned copper, Journal Of Applied Physics 115 (2) (2014).
[44] N. Li, J. Wang, J.Y. Huang, A. Misra, X. Zhang, Influence of slip transmission on the migration of incoherent twin boundaries in epitaxial nanotwinned Cu, Scripta Materialia 64 (2) (2011) 149–152.
[45] N. Li, J. Wang, X. Zhang, A. Misra, In-situ TEM Study of Dislocation-Twin Boundaries Interaction in Nanotwinned Cu Films, Jom 63 (9) (2011) 62–U62.
[46] J. Wang, N. Li, O. Anderoglu, X. Zhang, A. Misra, J.Y. Huang, J.P. Hirth, Detwinning mechanisms for growth twins in face-centered cubic metals, Acta Materialia 58 (6) (2010) 2262–2270.
[47] J.A. Brown, N.M. Ghoniem, Structure and motion of junctions between coherent and incoherent twin boundaries in copper, Acta Materialia 57 (15) (2009) 4454–4462.
[48] Q. Li, S. Xue, J. Wang, S. Shao, A.H. Kwong, A. Giwa, Z. Fan, Y. Liu, Z. Qi, J. Ding, H. Wang, J.R. Greer, H. Wang, X. Zhang, High-Strength Nanotwinned Al Alloys with 9R Phase, Advanced Materials 30 (11) (2018) 1704629.
[49] S.I. Rao, P.M. Hazzledine, Atomistic simulations of dislocation–interface interactions in the Cu-Ni multilayer system, Philosophical Magazine A 80 (9) (2000) 2011–2040.
[50] A. Misra, J.P. Hirth, H. Kung, Single-dislocation-based strengthening mechanisms in nanoscale metallic multilayers, Philosophical Magazine a-Physics Of Condensed Matter Structure Defects And Mechanical Properties 82 (16) (2002) 2935–2951.
[51] D. Tabor, The physical meaning of indentation and scratch hardness, British Journal of Applied Physics 7 (5) (1956) 159.
[52] Y.P. Li, X.F. Zhu, J. Tan, B. Wu, W. Wang, G.P. Zhang, Comparative investigation of strength and plastic instability in Cu/Au and Cu/Cr multilayers by indentation, Journal Of Materials Research 24 (3) (2009) 728–735.
[53] J. Wang, C. Yang, P.D. Hodgson, Extrinsic size effect in microcompression of polycrystalline Cu/Fe multilayers, Scripta Materialia 69 (8) (2013) 626–629.